Near-Field Measurement Based Prediction of Antenna Test Results Below 30 MHz in CISPR 25 Setups

Zongyi Chen, Stephan Frei
TU Dortmund University
Dortmund, Germany
zongyi.chen@tu-dortmund.de

***Abstract*—In automotive radiated emission testing, as specified in CISPR 25, the absorber lined shielded enclosure (ALSE) method is commonly used. This requires an expensive chamber. Based on the observation that the dominating coupling is capacitive at frequencies below 30 MHz, the emission tests often suffer from low reproducibility. In order to predict emission in an alternative test method, a Huygens's principle based field prediction method is presented in the paper. This method only requires a set of near-field measurements along a line above the metal table of the CISPR 25-setup. The uncertainties of the predicted fields at the measurement antenna location is reduced, because the near-field measurements dramatically minimize the influences from nearby objects. The higher field strength close to the cable also improve the signal to noise ratio with respect to external noises such that the method can be applied without the use of a shielded chamber. The proposed method defines an open Huygens's surface located in front of the cable harness and the equipment under test (EUT). First, the near-field measurements are conducted using an electrically-short monopole field probe, and second, the field distribution along the whole Huygens's surface can be found using the measured data and applying an appropriate extrapolation function over the Huygens's surface. The field distribution on this surface is finally used to calculate the electric field at the antenna location.**

Keywords——CISPR 25 setup; Near-field measurements; Huygens's principle; Field prediction below 30 MHz

I. INTRODUCTION

Electric automotive components and modules are required to pass radiated emission tests. According to the absorber-lined shielded enclosure (ALSE) method (CISPR 25, [1]), the equipment under test (EUT) with attached cable harness must be placed above a metal table and the tests performed inside an anechoic chamber. A measurement antenna is located at one meter distance in front of the test setup for detecting the radiated fields. Monopole, biconical, or log-periodic antennas are used, depending on the frequency range of interest. Considering that such expensive and space-consuming chambers are not always available, alternative methods are desired.

Various papers have discussed alternative methods to a typical CISPR 25 ALSE test setup. These papers rely mainly on the identification of Hertizian dipoles for radiation prediction. As the cable harness dominates the radiation below a few hundred MHz, a current probe is used to measure the common-mode currents along the cable harness. By introducing a multi-dipole model, and by fitting the measured currents into the model, the radiated field can be directly calculated. Such multi-dipole models for field prediction are analysed for example in [2]-[5]. This approach can accurately predict fields above 30 MHz. However, below 30 MHz the method does not work properly, because it is too sensitive to unavoidable phase errors of the common-mode currents along the cable harness [4].

An approach for improving the field prediction below 30 MHz is discussed in [6]. The method uses measurement-based transfer functions without phase information. It is shown that it provides a good field prediction for a fixed shielded cable setup with fixed termination impedances similar to the ones used in the generation of the transfer impedances. However, once the termination impedances differ strongly from the impedances used for the transfer function generation the method fails to predict the fields. A set new transfer functions is required to obtain good matching results.

This paper focuses on improving field prediction below 30 MHz. As depicted in Fig. 1(a) for a simplified standard test setup below 30 MHz, the EUT is connected with a cable harness of 1.5 m length. When conducting field measurements, the EUT is connected to a power supply through an artificial network (AN). The radiated field is measured with a 1-m-long vertical monopole antenna locating at 1 m distance (D = 1 m). The detected antenna voltage combined with the antenna factor provides the electric field at the antenna location. Fig. 1(b) depicts the proposed Huygens's principle based field prediction method. Using Huygens's principle to create a transfer function between the near-field distribution and the predicted antenna voltage has been shown only in simulation in [9]. Distinguished from [9], the proposed method defines an open Huygens's surface (see Fig. 1(b)). The proposed method only needs near-field measurements to be conducted at several locations along a line above the metal table (represented by red arrows). The measured data is first applied with an interpolation function to obtain the interpolated fields (represented by blue arrows), and then, a proper extrapolation formula is used to give field distributions for the rest points over the defined Huygens's surface (represented by green arrows). With this information, the electric field at antenna location can be simply calculated through the known field distributions along the whole defined Huygens's surface.

978-1-5090-1416-3/16/$31.00 ©2016 IEEE

While performing near-field measurements, a shielded chamber is normally not required. Here, however, the proposed measurement is depicted inside a chamber (see Fig. 1(b)) for

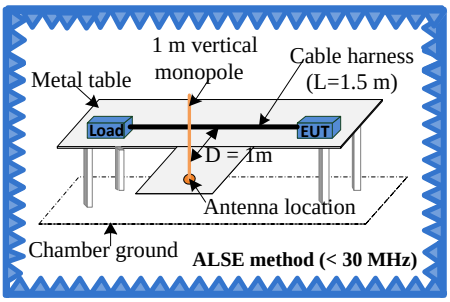

(a)

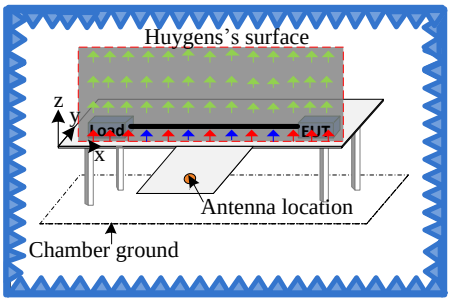

(b)

Fig. 1. Test setup. (a) Standard test setup (ALSE method below 30 MHz), (b) Huygens's principle based field prediction method

two reasons. The first reason is to highlight the difference compared to the standard test setup. Because the motivation for the new method is to reduce measurement uncertainties through near-field measurements, as uncertainties increase at frequencies below 30 MHz are discussed in [7-8]. By conducting near-field measurements, the coupling from chamber walls and other equipment can be largely minimized. Therefore, the uncertainties of the predicted field, compared to the standard field measurement, can be reduced. The second reason is the consideration of signal to noise ratio of the measured field strength. Even though the near-fields are measured very close to test setup, if the measurement environment is very noisy, a small shielded chamber may be needed.

The proposed method is described in detail in the following sections. Section II describes the open Huygens's surface, Section III analyses field components over the defined Huygens's surface, and presents the field approximation method. Section IV validates the proposed method. The predicted field at one meter distance is compared with standard chamber measurements.

II. Application of Huygens's Principle

If the Huygens's principle [10] is applied consequently a closed fictitious surface (so-called Huygens's surface) is needed to wrap the real radiation structure. Then equivalent current sources placed on the Huygens's surface can replace the fields generated by the original radiating structure in the outer region of the Huygens's surface. However, as it's too difficult to measure the field distributions over a large closed surface the method is not suitable as alternative method to the standard ALSE method. A simplification of the Huygens's surface is necessary.

The proposed method simplifies the problem threefold. First, an open Huygens's surface is used instead of the typical closed surface. It is placed between the table and the field prediction point. Second, the field is only measured at the surface of the table and extrapolation functions are used to estimate the field on the surface, greatly reducing the number of field measurement points. Finally, only the E_z component is used.

A. *Definition of an Open Huygens's Surface*

In Fig. 1(b), a rectangular plane, perpendicular to the metal table, located in the front of the test setup is visualized. As the plane is placed between the table and the field observation point, it is reasonable to assume that the electric field at the antenna location is dominated by the equivalent sources on the reduced Huygens's surface. Using the E- and H-field distributions over the reduced Huygens's surface, the equivalent current sources can be determined through (1) and (2). The electric field at antenna reference point can be obtained by integration through (3).

$$\vec{J_s} = \vec{n} \times \vec{H_s} \tag{1}$$

$$\vec{M_s} = -\vec{n} \times \vec{E_s} \tag{2}$$

$$\vec{E}(\vec{r}) = \iint [-j\omega\mu\vec{J_s}G(\vec{r},\vec{r'}) + \vec{M_s} \times \nabla'\vec{G}(\vec{r},\vec{r'}) - \frac{1}{j\omega}(\nabla' \cdot \vec{J_s})\nabla'\vec{G}(\vec{r},\vec{r'})]ds' \tag{3}$$

B. *Validation of the Reduced Huygens's Surface Approach*

Fig. 2 shows a simplified test setup used to verify the correctness of the reduced Huygens's surface. The model was created and simulated using CONCEPT-II [11]. In order to save simulation time and to reduce model complexity, the metal table (see Fig. 1) was replaced by an infinite perfect electric conductor (PEC) ground plane. Only a single unshielded wire was used to represent the attached cable harness. The ANs were not involved.

As shown in the Fig. 2(a), the reduced Huygens's surface (dashed red outline) has the following dimensions: 3 m long, 1 m high, and the bottom of the surface touches the PEC ground. The wire is 1.5 m long. Both ends of the wire have the same distance to the edge of the Huygens's surface. The antenna is located at a distance of 1 m from the center of the wire. A source V_S having a source impedance of Z_S = 50 Ω is used. Z_L varied between 10 Ω, 50 Ω, 330 Ω, 10 kΩ for investigating the effect of different termination impedances. The Huygens's surface is located 5 cm in front of the simplified test setup (see Fig. 2(b)). The simulated vertical polarized electric fields at the antenna location are shown in Fig. 3. For all simulated termination impedances, Huygens's principle-based predicted fields are shown by dashed lines. They are calculated using equations (1)-(3). All fields on the defined Huygens's surface are from simulation model, and E_x, E_z, H_x and H_z are used. The solid lines show the full-wave simulation results from CONCEPT-II. Both results match, indicating the correct implementation of

Huygens's principle, and supporting the simplification of only using a plane.

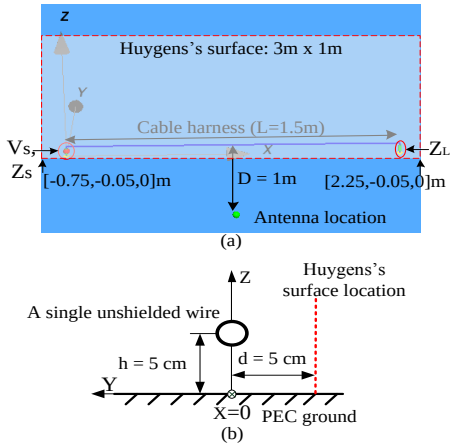

Fig. 2. Simplified test setup in CONCEPT-II. (a) A single unshielded wire over PEC ground, driven by an ideal voltage source Vs, with source impedance Z_S and load impedance Z_L, also the location of the defined Huygens's surface. (b) Side view, shows relative position of wire and the defined Huygens's surface.

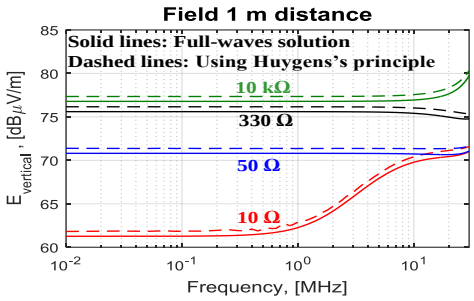

Fig. 3. Huygens's surface applies for different load impedances

III. Field Distributions Over Huygens's Surface

To predict the electric field at the antenna location the field distributions along the whole surface needs to be known. However, conducting E-field measurements in free space is difficult and time consuming. The proposed method simplifies further by using only the measure E_z at a few locations. To obtain the fields on the surface from the measured data, a proper field extrapolation method will be introduced.

A. Field Components

Using the coordinate system as defined in Fig. 1(b), the tangential field components on the Huygens's surface are E_z and H_z, E_x and H_x. In order to determine which tangential field component has the largest contribution to the field at the antenna location the simplified test setup shown in Fig. 2 was used and the load impedance (Z_L = 50 Ω) was chosen. The other impedance cases (10 Ω, 330 Ω, 10 kΩ) were also simulated showing similar results with respect to the dominating contribution. Fig. 4 shows the $E_{vertical}$ at the antenna location contributed from different field components over the Huygens's surface (Z_L = 50 Ω). It shows that the E_z field component dominates. Only using E_z the observed error is about 5 dB relative to a full-wave simulation. The contribution from E_x is too weak, thus it's neglected and not shown in the figure. The observed magnetic field components (H_x and H_z) have smaller

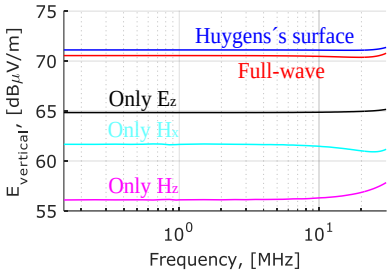

Fig. 4. Contribution from different field components

contributions than E_z component. Thus, the method simplifies further by using only the E_z fields. The improvement by adding field contribution from H_x and H_z are analysed in the discussion section.

B. Field Approximation

As the proposed method only measures E_z at several locations above metal table, no phase information is captured. A spline function [12] is introduced for field interpolation. The ideal is also represented in Fig. 1(b) where blue arrows representing the interpolated field points. This interpolation is required because, as discussed in [13], sufficient near-field data is required for the far-field transformation.

The next processing step is to extrapolate E_z for the remainder of the points over the defined Huygens's surface. This can be done by using an electrostatic approximation, as described in e.g. [14]:

$$E_z = \frac{V_p}{\ln(2h/r)}\left[\frac{z-h}{(z-h)^2+y^2} - \frac{z+h}{(z+h)^2+y^2}\right] \quad (4)$$

The corresponding cable and observation point P are shown in Fig. 5.

Comparisons between full-wave simulation and fields calculated using equation (4) are shown in Fig. 6 at position x = 0.25 m for frequencies 150 kHz (upper) and 30 MHz (lower) respectively. The field extrapolation delivers missing field values along the Huygens's surface. In the Fig. 6, the stars along the curves represent positions where fields are compared, and only E_z magnitude distributions are shown.

As in the measurement, phase information of E_z will not be captured, we simply assume the phase of the measured E_z and interpolated E_z are of 0°. This assumption is proper because the considered frequency range is only up to 30 MHz. However for observation points at different heights along the Huygens's surface, a phase shift of 180° can be observed due to the cable structure itself (see Fig. 5), this can be also obtained for the extrapolation equation (4). This 180° phase shift from equation (4) is also added to the extrapolated fields.

It can be seen that using an electrostatic approximation is acceptable in this frequency range of interest. Thus, the curve from equation (4) (see Fig. 6, red curve) can be used for the approximation of field distributions along Huygens's surface. By applying only magnitude of measured E_z and interpolated E_z as start value to the curve, and shifting the curve up and down

according to the start value, the fields along the defined Huygens's surface can be obtained. Thus, through equation (1)-(3), the electric field at antenna location can be predicted.

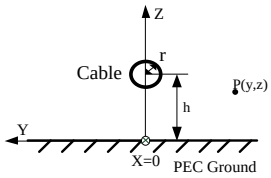

Fig. 5. A cable above PEC ground for field extrapolation

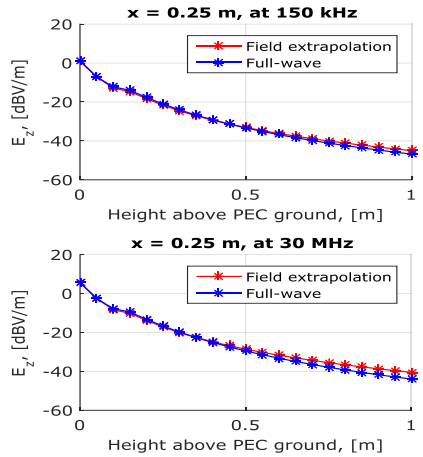

Fig. 6. Comparison of E_z along the height of Huygens's surface between field extrapolation and full-wave simulation for at 150 kHz and 30 MHz

IV. Method Validation

In order to test the proposed method, near-field measurements have been carried out for a CISPR 25 test setup, as shown in Fig. 7. A 1.5 m long TWP-cable represents the cable harness. A floating PCB represents the EUT. According to the standard, two ANs are used. Fig. 7(a) shows the schematic. Fig. 7(b) shows a photo of the setup. The electrically-short field probe (with R&S EZ-12 impedance converter) which was used to measure the near-field is shown in front of the TWP-cable. The field probe is 3.5 cm long, and placed at a distance of 5 cm to the cable (see Fig. 7(c)). A tracking generator (R&S ESRP, 10 Hz ~ 7 GHz) with an output power of 0 dBm is used. The PCB has a size of 20 cm x 15 cm, and detailed in Fig. 7(d) is a top view. A simple circuit over the upper layer of the PCB, consists of two copper tape traces with a 2 cm gap and a 50 Ω termination, and each copper tape has a length of 15 cm. The bottom layer is of copper facing the metal table and above metal table 5 cm (see Fig. 7(e)).

A. Near-field Measurements

1) Field probe calibration

Before conducting near-field measurements, the field probe (see Fig. 7(c)) needs to be calibrated. Small electric-field probes can be calibrated using a TEM cell. However, the size of the antenna impedance converter significantly disrupts the E-field distribution inside the TEM cell. Instead a small calibration structure is used to calibration the field probe, shown in Fig. 8. In contrast to a TEM cell it is not possible to calculate the field analytically for this structure. For that reason a numerical solution is used to determine the field at the probe's location. The probe factor (P_f) can be simply defined by:

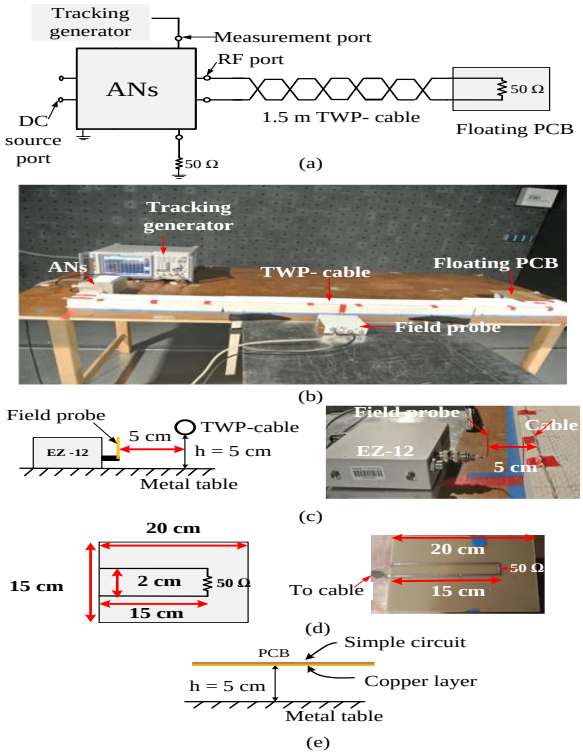

Fig. 7. Measurement setup, (a) Schematic, (b) Photo, (c) Distance from the field probe to the cable, (d) Simple circuit over PCB (top view), (e) PCB above the metal table (side view)

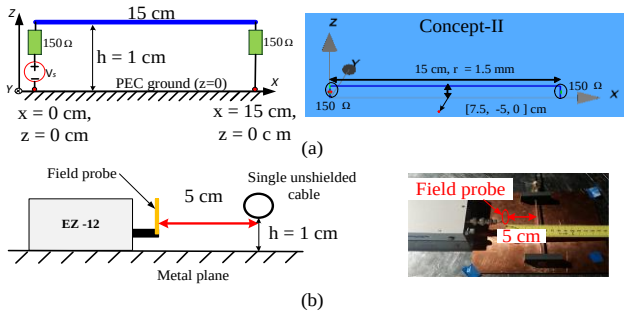

Fig. 8. Field probe antenna calibration, (a) Calibration model in simulation, (b) Field probe in calibration

$$P_f = \frac{E_{simu}}{V_{ant}} \quad (5)$$

where V_{ant} is the output voltage of the antenna impedance converter when the field probe is placed into the calibration structure, E_{simu} is the field at the observation point obtained from the simulated calibration structure.

In Fig. 8 (a), the left figure shows a sketch of the calibration structure, it consists of an unshielded cable of 15 cm length placed 1 cm above PEC ground, the radius of the cable is 1.5 mm, both source and load impedances are 150 Ω. The field observation point is at [7.5, -5, 0] cm, which is 5 cm distant to the cable, and directly over the PEC ground. Only E_z (= E_{simu}) has to be considered for calibration. Meanwhile, the field probe is placed 5 cm away from the cable in the calibration structure

(see Fig. 8 (b)), and then, the V_{ant} can be obtained. Applying equation (5), the probe factor can be determined.

2) E-field measurements

The measured electric field along different locations of the cable is shown in Fig. 9. For a better description, Fig. 9(a) shows a top view of the setup. The cable starts at 0 m and ends at 1.5 m. The red dashed line shows the path which the short monopole antenna (3.5 cm long) moves along with. The corresponding electric field distributions along the path are shown in Fig. 9(b), as an example, only results at 150 kHz, 1 MHz, 10 MHz, and 30 MHz are illustrated. The star markers give the positions where field are measured. It shows the dominating fields are caused by the cable harness. Away from the cable harness, the field intensity is reduced, as shown in the figure, only 20 cm distance causes around 20 dB decrease. Considering the real measurement dynamic range, we assume only the electric fields along the path and inside of the length of metal table are related to electric field at antenna location, and the fields outside are assumed to be zero. Therefore, the Huygens's surface can also be located along the path, and vertical to the metal table. The length of the Huygens's surface can be limited to 2 m (metal table length), the height of Huygens's surface has been set to 1 m.

When conducting E-field measurements, if a test receiver with a fast time domain scan is introduced, e.g. R&S ESRP, the total measurement time would not be a problem. And the numerical post-processing for electric field calculation at 1 m distance only need several seconds. The E-field measurements based method is highly applicable.

B. Electric Field at 1 m Distance

To validate the proposed method, field measurement according to standard was performed as comparison.

1) Standard field measurements

According to the standard, the field measurement was conducted inside a shielded chamber, as shown in Fig. 10. The 1-m-long vertical monopole antenna (Schwarzbeck, FMZB 1513) is located at 1 m distance and facing the TWP-cable. The manufacturer provided antenna factor was applied for calculating the electric field at the antenna location.

2) Analytical calculation

In order to analytically estimate the electric field at 1 m distance. The analytical formulas in [15] (at page 2, formula (1)-(3)) are used. These equations need both currents and voltages at both ends of the transmission line. To apply the equations, the TWP-cable involved in the setup was considered to be two unshielded transmission lines in parallel carrying a differential current. An equivalent circuit model in Fig. 11 illustrates the model, including the model for ANs, distributed line elements for the TWP-cable, and a simple model representing the floating PCB. This is only a rough model based on empirical rule. After circuit simulation, the current and voltage on the both ends of cable can be obtained, and then, the field at 1 m distance can be calculated.

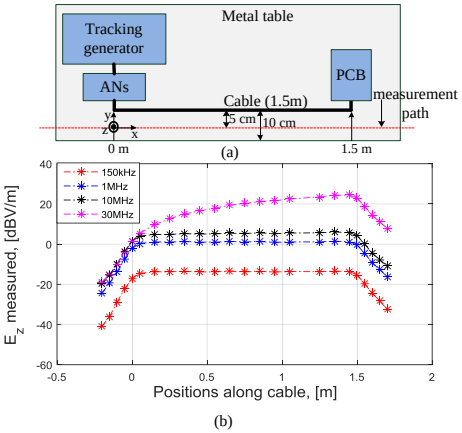

Fig. 9. Near-field measurements, (a) Measurement path, (b) Measurement results

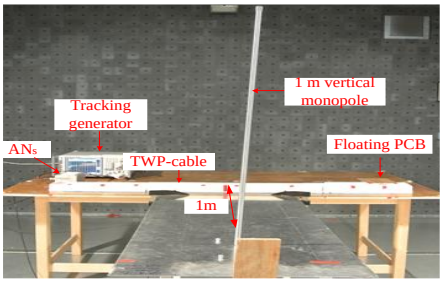

Fig. 10. Standard antenna measurement setup

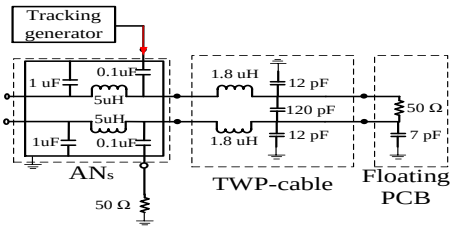

Fig. 11. Equivalent circuit model of setup over metal table

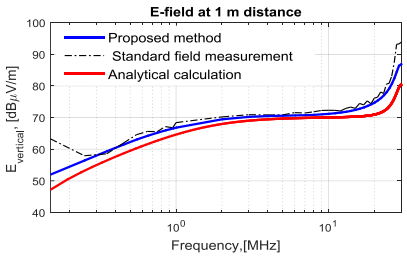

Fig. 12. Comparisons of electric field at 1 m distance

3) Field comparison

Fig. 12 shows the electric field comparison at 1 m distance. The blue curve is the calculated field using the proposed method. The black curve is the result from the standard field measurement. The red curve is analytical formula based estimation result. It can be seen all three curves show good similarity. The results calculated using the proposed method matches the standard field result very well for most frequencies. The deviation observed in analytical calculation, compared

with the standard field measurement, may be caused by insufficient parameters in the circuit model.

V. Discussion

The proposed method uses only measured E_z-fields at different positions (see Fig. 13), magnetic field components were not considered, but they can contribute to the electric field at 1 m distance. For investigating the effect of the magnetic fields, an H-field probe (Langer EMV) was used to measure the magnetic field close to the TWP-cable, shown in Fig.13. The field was only measured at one point. The point was selected close to the PCB (see Fig. 13(a)). The detected probe power is represented in Fig. 13(b), where beneath 10 MHz, the signal is very weak, may be caused by limited dynamic range of the used probe. Therefore, in the paper, the influence from H-field components is shown starting from 10 MHz. Currents along the cable harness can be calculated based on the measured H-field component. And then, the multi-dipole model can be used to obtain the contribution by the magnetic field. Here it is assumed, that the currents are uniformly distributed without phase changes along the TWP-cable. Fig. 13(c) shows the result. The combination of the E_z field with the H_x field contribution (magenta curve) or with both the H_z and H_x field contribution (cyan curve)shows that the predicted electric field, increased by 1~3 dB.

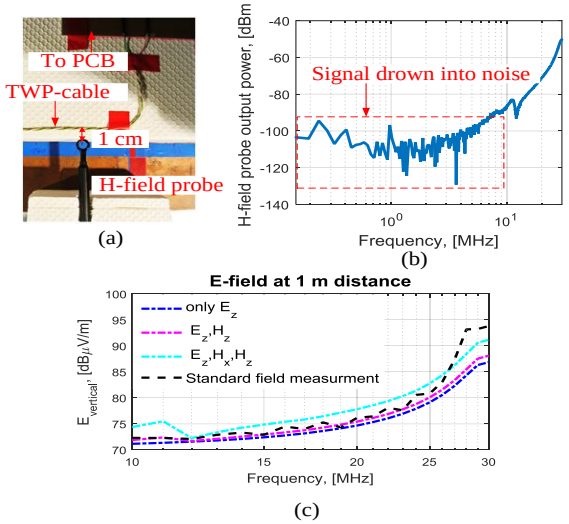

Fig. 13. H-field measurement as compensation

VI. Conclusion

A Huygens's principle based field prediction method was developed for a CISPR-25 test setup below 30 MHz. An open Huygens's surface was defined located in the front of the cable harness 5 cm. The field component on the Huygens's surface which contributes mostly to the vertical electric field at the observation point is the E_z field component independent of the termination impedance of the wire harness. For that reason an electric field probe oriented along the z-axis and placed on the metal surface is sufficient to capture the primary field component. Using field extrapolation in the vertical direction and interpolation between measurement points in the horizontal direction the distribution of the primary field component over the entire Huygens's surface can be estimated. Therefore the electric field at 1 m distance can be calculated. Using near field measurements offers a set of advantages: (1) due to the much larger field strengths in the near field a shielded room is only needed if the surrounding is very noisy, (2) detrimental effects of typical absorber rooms, such as the loss of the absorber performance at low frequencies, resulting chamber resonances etc. do not affect the near field data, as this is dominated by the harness voltage and current.

Therefore the paper proposes an alternative method to chamber measurements below 30 MHz and gives in-sight into the effects of simplifications when using Huygens's principle for field prediction.

References

[1] CISPR 25 Ed.4.0: "Vehicles, boats and internal combustion engines-Radio disturbance characteristics – Limits and methods of measurements for the protection of on-board receivers," 2015.

[2] J. Jia, D. Rinas, and S. Frei, "An alternative method for measurement of radiated emissions according to CISPR 25," *IEEE Int. Symp. Electromagn. Compat.*, Brugge, 2013, pp. 304-309.

[3] D. Schneider, M. Bottcher, B. Schoch, S. Hurst, "Transfer functions and current distribution algorithm for the calculation of radiated emissions of automotive components," *IEEE Int. Symp. Electromagn. Compat.*, Brugge ,2013, pp. 443-448.

[4] J. Jia, Current Scan Methods to Predict Radiated Emissions of Automotive Components According to CISPR 25, Ph.D. dissertation, On-board system lab, TU Dortmund., Dortmund, Germany, 2015.

[5] J. Jia, D. Rinas, S. Frei,''Prediction the radiated emission of automotive sytems according to CISPR25 using current scan methods'' *IEEE Trans. Electromagn.Compat.*, vol. PP, no. 99, pp. 1–10, Jan. 2016.

[6] D. Schneider, M. Beltle, B. Siegel, S. Tenbohlen, and W. Kohler, "Radiated emissions of an electric drive system estimated on a bench using disturbance currents and transfer functions," *IEEE Trans. Electromagn.Compat.*, vol. 57, no. 3, pp. 311–321, Mar. 2015.

[7] C.W. Fanning, "Improving Monopole Radiated Emission Measurement Accuracy; RF Chamber Influences, Antenna Height and Counterpoise Grounding (CISPR 25 & MIL-STD-461E vs MIL-STD-461F)," *IEEE Int. Symp. Electromagn. Compat.*, Austin, TX, 2009, pp. 103-118.

[8] F.-J. Bongartz, J. Deckers, M. Heina, H. Hirsch, J. Mooser, J.-C. Nickel, and M. Seiger, "Proposal for the validation of absorber lined shielded enclosures for CISPR 25 emission tests," in Proc. *IEEE Int. Symp. Electromagn. Compat.*, Austin, TX, 2009, pp. 116–120.

[9] A Radchenko, V. Khilkevich, N. Bondarenko, D. Pommerenke, M. Gonser, J. Hansen, and C. Keller, "Transfer function method for predicting the emissions in a CISPR 25 test-setup," *IEEE Trans. Electromagn. Compat.*, vol. 56, no. 4, pp. 894-902, Aug. 2014.

[10] C. A.Balanis, Advanced Engineering Electromagnetics. NewYork, NY, USA: Wiley, 1989.

[11] CONCEPT-II-12.0, Technische Universität Hamburg-Harburg. (2015). [Online]. Available: *http://www.tet.tuhh.de/en/concept/*.

[12] de Boor, C., A Practical Guide to Splines, Springer-Verlag, 1978.

[13] M. Sorensen, O. Franek, G. Pedersen, A. Radchenko, K. Kam and D. Pommerenke, "Estimate on the uncertainty of predicting radiated emission from near-field scan caused by insufficient or inaccurate nearfield data: Evaluation of the needed step size, phase accuracy and the need for all surfaces in the huygens' box", *IEEE Int. Symp. Electromagn. Compat*., pp. 1-6, 2012.

[14] Z. Li, Electromagnetic Sensors for Measurements on Electric Power Transmission Lines, Ph.D. dissertation, Washington States University. August 2011.

[15] J. Jia, F. Kremer, S. Frei, "Modellierung von CISPR-25 Antennenmessungen mittels schneller approximierender Berechnungsverfahren", EMV-Düsseldorf, Germany, 2012